doi:10.1038/nature11447

1. Luminosities of the surviving companions

As stated in the main text, hydrodynamic simulations[22] of the interaction of the SNIa ejecta with either a main-sequence or a subgiant companion predict a significant injection of energy into the outer layers of the companion star that remain gravitationally bound after the impact. That results in a large excess in radius and in luminosity of the companion, as compared with the values corresponding to its mass and evolutionary stage, in hydrostatic and thermal equilibrium (the estimate is as high as $\sim$5,000 $L_\odot$). Simulations[23] of the collision of the material ejected by a SNIa with a main-sequence companion are entirely consistent with earlier ones[22], the differences in the amount of mass stripped from the companion being due only to the more compact initial stellar models adopted for the simulations. The question still remains of how fast thermal equilibrium is restored (hydrostatic equilibrium is recovered very shortly after the collision with the SNIa ejecta). This issue has been explored for the case of main-sequence and subgiant companions[24]. Contrary to the assumption[22] that the governing time scale for the evolution in luminosity should be the thermal time scale of the whole stellar envelope, it is found that the luminosity can decrease much faster, due to the short cooling times of the outermost layers, so that in a much reduced time it could return (roughly) to its pre-explosion value.

The luminosity evolution depends on the amount of mass stripped, on the energy injected into the bound layers and on the cooling times of the outermost part of the stellar envelope. For values matching the results of the hydrodynamic simulations[22] (and for a subgiant companion), the luminosities predicted[24] for a time $\sim$1000 yr after the SNIa explosion are within $\sim$10–25$L_\odot$. Thus, even allowing for a wide margin of uncertainty, nothing below solar luminosity is to be expected.

A possibility has been suggested, within the SD channel, involving a low luminosity companion of the exploding white dwarf at the time of the SNIa[31,32]. The idea is that mass transfer from the companion spins up the accreting white dwarf, making the critical mass for explosive carbon ignition, $M_{\rm crit}$, higher than the Chandrasekhar mass ($M_{\rm Ch} \simeq 1.4\ M_\odot$). If mass transfer ceases when the mass of the white dwarf, M, is still lower than the $M_{\rm crit}$ corresponding to its spin rate (but higher than $M_{\rm Ch}$), there should be some time interval τ between the end of mass accretion and the SNIa, required for spinning down until $M_{\rm crit} = M$. It is then speculated[32] that τ could be long enough for the companion (if it were a red giant or even a subgiant star) to have become a white dwarf. It must be noted that solid-body rotation only very slightly increases $M_{\rm crit}$ above $M_{\rm Ch}$ ($M_{\rm crit} = 1.47\ M_\odot$). Only differential rotation can significantly increase $M_{\rm crit}$[33,34], but, in any case, the upper limit to the time scale for angular momentum redistribution and loss appears to be $\sim 10^6$ yr only[33]. That would be enough, if the mass donor were a red-giant star and mass transfer stopped owing to contraction of the envelope when its mass becomes too low to sustain the red-giant structure[31], to have a companion with a radius much smaller than the Roche lobe radius, but it would not be much less luminous than during the previous stage yet. To assume arbitrarily long time scales for angular momentum redistribution and loss (thus allowing the companion star to become a white dwarf) is not supported by current models[35,36].

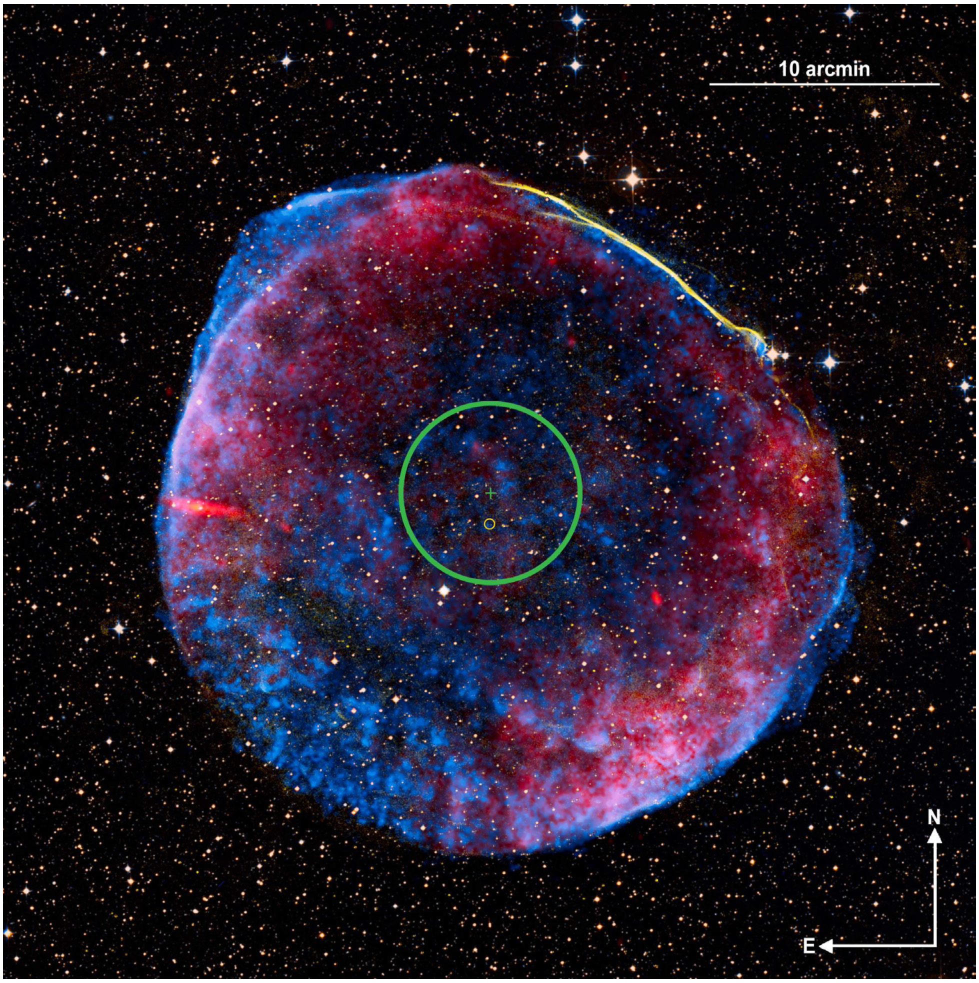

Figure S1 | The remnant of the SN1006 The surveyed area is indicated by the large green circle. The centre of the survey (the centroid of the X-ray emission) is marked with a green cross, and that of the Hα emission, by the small yellow circle. This is a composite image of the SN 1006 supernova remnant, which is located about 7000 light years from Earth. Shown here are X-ray data from NASA's Chandra X-ray Observatory (blue), optical data from the University of Michigan's 0.9 metre Curtis Schmidt telescope at the NSF's Cerro Tololo Inter-American Observatory (CTIO; yellow) and the Digitized Sky Survey (orange and light blue), plus radio data from the NRAO's Very Large Array and Green Bank Telescope (VLA/GBT; red). Image credit: X-ray: NASA/CXC/Rutgers/G.Cassam-Chenaï, J.Hughes et al.; Radio: NRAO/AUI/NSF/GBT/VLA/Dyer, Maddalena & Cornwell; Optical: Middlebury College/F.Winkler, NOAO/AURA/NSF/CTIO Schmidt & DSS

2. Distance determinations of the sample stars

We have estimated the distances of the sample stars from the photometric magnitudes in five different filters: Johnson m_B and m_R, and m_J, m_H and m_K from the 2MASS[19] catalogue (see Supplementary Table S2). The masses of the stars were estimated using a code[37,38,39] kindly provided by C. Allende-Prieto, according to their stellar parameters: effective temperature, $T_{\rm eff}$, and surface gravity, $\log g$, and their metallicity, [Fe/H], and assuming for all stars the uncertainties of 100 K, 0.3 dex and 0.1 dex in $T_{\rm eff}$, $\log g$ and [Fe/H], respectively. The calculations are based on solar-scaled theoretical isochrones[40]. The radii were then derived from the surface gravity and mass. This radius, together with the spectroscopic estimate of the effective temperature, provides the intrinsic bolometric luminosity in the ranges $0.3 < L_\star/L_\odot < 1.4$ for dwarfs, $4 < L_\star/L_\odot < 14$ for subgiants, and $19 < L_\star/L_\odot < 69$ for giants.

In the Supplementary Table S3, we show the distance determinations for the different filters, using the bolometric corrections for models without overshooting[41], for our preferred value of the colour excess, $E(B-V) = 0.096$ mag, and other sets of the relevant parameters. We compute the magnitude corrected for extinction in each filter as $m_{V,0} = m_V - A_V$, where $A_V = 3.12\,E(B-V)$ is the extinction in the Johnson V filter. We adopt the following values for other filters[42]:$A_B/A_V = 1.31$ $A_R/A_V = 0.84$, $A_J/A_V = 0.32$, $A_H/A_V = 0.27$ and $A_K/A_V = 0.21$. We adopt errors in m_B and m_R of 0.03. The error in the distance from each filter takes into account uncertainties of 100 K and 0.3 dex in the stellar parameters, and uncertainties of 0.2 $M_\odot$ and 0.05 in mass and reddening, respectively, plus the individual errors of the photometric magnitudes. The final average distance of each star is given in Table 1, and Supplementary Tables S2 and S3 give the mean distances weighted by the individual uncertainties in different filters. We note that distance determinations from different filters are consistent and the final errors in the distances mostly reflect the systematic uncertainties.

The possibility that the proposed companion, Tycho G, of the SNIa SN 1572 had lost part of its envelope, $\Delta M = -0.2$ $M_\odot$, due to the impact of the supernova ejecta[22,23,24], and that that would affect its derived distance, has been discussed[9]. It was concluded that the lower mass does not produce a significant change in the derived average distance, assuming that the subgiant companion star is able to almost completely recover thermal equilibrium between $\sim 10^2$ and $\sim 10^3$ yr after the white dwarf explosion[24]. We have done similar calculations and checked that this statement also applies to the sample stars in the SN 1006 field.

Finally, we inspected the 2MASS[19] catalogue to search for any possible main-sequence candidate to be the companion of SN 1006. For that, we extracted the 2MASS JHK magnitudes of the stars within the 4 arcmin radius around the centre of SN 1006 and computed the effective temperature from the IRFM[43] assuming that all stars in the field are solar-metallicity ([Fe/H]= 0), main-sequence ($\log g = 4.5$) stars. We determined their masses and luminosities as previously indicated and saw that there are only roughly 15 stars with magnitudes m_R in the range 16.3–17.5 (m_K in the range 15.1–15.7) and $T_{\rm eff}$

in the range 5250–6450 K. The same exercise has been repeated for slightly evolved stars, with $\log g = 4$. In this case, there are just 3 stars with magnitudes m_R in the range 16.0–16.3 (m_K in the range 14.8–15.1) and $T_{\rm eff}$ in the range 5350–5500 K. This upper-limit in the apparent magnitude corresponds to an absolute magnitude of $M_R = +4.1$. The case for $\log g = 3.5$ produces stars at distances far beyond that of SN 1006. Therefore, as stated in the main text, any possible main-sequence companion at the distance of the SNR should be about as luminous as the Sun or less. Slightly evolved companions should have roughly twice the solar luminosity at most.

3. Determination of stellar parameters and element abundances of the sample stars

The stellar atmosphere parameters of the sample stars were obtained from the Fe I and Fe II excitation and ionization equilibria. We derive the equivalent widths (EWs) of the Fe I and Fe II lines with the ARES code[44] using a line list with 263 Fe I and 36 Fe II lines[45]. The parameters were computed using the StePar code[25]. This code employs the 2002 version of the MOOG code[26], and a grid of Kurucz ATLAS9 plane–parallel model atmospheres[27]. Our analysis has been performed assuming local thermodynamic equilibrium (LTE). The parameters are shown in columns 2–4 of Table 1.

The chemical abundances have been derived by computing the EWs of spectral lines using the ARES code[44] for all the elements. Once the EWs are measured, we use the LTE MOOG code[26] to compute the chemical abundance provided by each spectral line, using the appropriate ATLAS9 model atmosphere[27] for each star. We determine the mean abundance of each element relative to its solar abundance (using the UVES spectrum of the Moon) by computing the line-by-line mean difference. In Supplementary Tables S4a and S4b, we provide the average abundances of each element, together with the errors associated with the dispersion of the measurements from different spectral features. In Fig. 3 and Supplementary Fig. S3 we compare the abundance ratios [X/Fe] with the Galactic trends[20] and we do not see any clear signature of enhancement in the abundances of α-elements or Fe-peak elements in any of the sample stars. The high scatter in the abundance ratios of some elements is related to the small available number of lines in the spectra.

Supplementary References

31 Justham, S. Single degenerate type Ia supernovae without hydrogen contamination. *Astrophys. J. (Letters)*, **730**, L34–L38 (2011)

32 Di Stefano, R., Voss, R., Claeys, J.S.W. Spin–up/spin–down models for Type Ia supernovae. *Astrophys. J.*, **738**, L1–L4 (2011)

33 Yoon, S., Langer, N. Presupernova evolution of accreting white dwarfs with rotation. *Astron. Astrophys.*, **419**, 623–644 (2004)

34 Yoon, S., Langer, N. On the evolution of rapidly rotating massive white dwarfs towards supernovae or collapses. *Astron. Astrophys.*, **435**, 967–985 (2005)

35 Saio, H., Nomoto, K. Off–center carbon ignition in rapidly rotating, accreting carbon–oxygen white dwarfs. *Astrophys. J.*, **615**, 444–440 (2004)

36 Piro, A.L. The internal shear of Type Ia supernova progenitors during accretion and simmering. *Astrophys. J.*, **679**, 616–625 (2008)

37 Allende-Prieto, C., Asplund, M., Fabiani Bendicho, P. S4N: A spectroscopic survey of stars in the solar neighborhood. The Nearest 15 pc. *Astron. Astrophys.*, **423**, 1109–1117 (2004)

38 Reddy, B. E., Lambert, D. L., Allende Prieto, C. Elemental abundance survey of the Galactic thick disc. Monthly Not. Royal Astron. Soc., **367**, 1329–1366 (2006)

39 Ramírez, I., Allende Prieto, C., Lambert, D. L. Oxygen abundances in nearby stars. Clues to the formation and evolution of the Galactic disk. *Astron. Astrophys.*, **465**, 271–289 (2007)

40 Bertelli, G., Bressan, A., Chiosi, C., Fagotto, F., Nasi, E. Theoretical isochrones from models with new radiative opacities. *Astron. Astrophys. Suppl.*, **106**, 275–302 (1994)

41 Bessell, M. S., Castelli, F., Plez, B. Model atmospheres broad-band colors, bolometric corrections and temperature calibrations for O - M stars. *Astron. Astrophys.*, **333**, 231–250 (1998)

42 Schaifers, K., *et al.* Astronomy and Astrophysics. C: Interstellar Matter, Galaxy, Universe, in Landolt–Börstein: Numerical Data and functional Relationships in Science and Technology. New Series (Springer–Verlag, Berlin) (1982)

43 González Hernández, J. I., & Bonifacio, P. A new implementation of the infrared flux method using the 2MASS catalogue. *Astron. Astrophys.*, **497**, 497–509 (2009)

44 Sousa, S.G., Santos, N.C., Israelian, G., Mayor, M., Monteiro, M.J.P.F.G. A new code for automatic determination of equivalent widths: Automatic Routine for line Equivalent widths in stellar Spectra (ARES). *Astron. Astrophys.*, **469**, 783–791 (2007)

45 Sousa, S.G. *et al.* Spectroscopic parameters for 451 stars in the HARPS GTO planet search program. Stellar [Fe/H] and the frequency of exo–Neptunes. *Astron. Astrophys.*, **487**, 373–381 (2008)

46 Gray, D. F. The observation and analysis of stellar photospheres. *Camb. Astrophys. Ser.*, **Vol. 20** (1992)

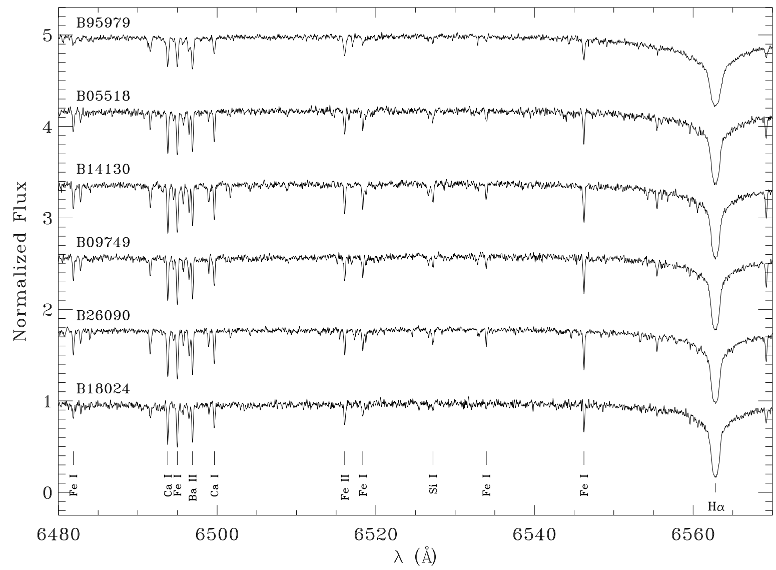

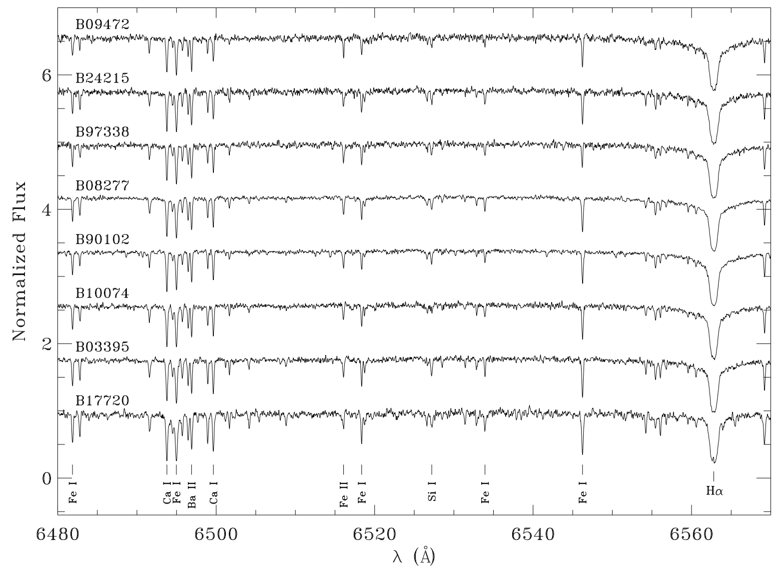

Figure S2 | Observed UVES spectra of the candidate dwarf stars. Spectra of the F-type (top panel) and G-type (bottom panel) sample stars, labelled by their names in Table 1, and sorted in decreasing effective temperature order from top to bottom. These high-resolution spectra were obtained at the 8.2-m Kueyen VLT (UT2) telescope equipped with UVES at the Cerro Paranal Observatory in Chile. They were obtained on 13, 14, 25, 28–30 April 2002 and on 1 May 2002, covering the spectral regions 3295–5595 Å, 5680–6645 Å, 6705–8515 Å, and 8675–10420 Å at resolving power $\lambda/\Delta\lambda \approx 43\,000$. The S/N of the spectra is in the range 50–170 and typically 80. The data were reduced in a standard manner, and later normalized within IRAF, using low-order polynomial fits to the observed continuum.

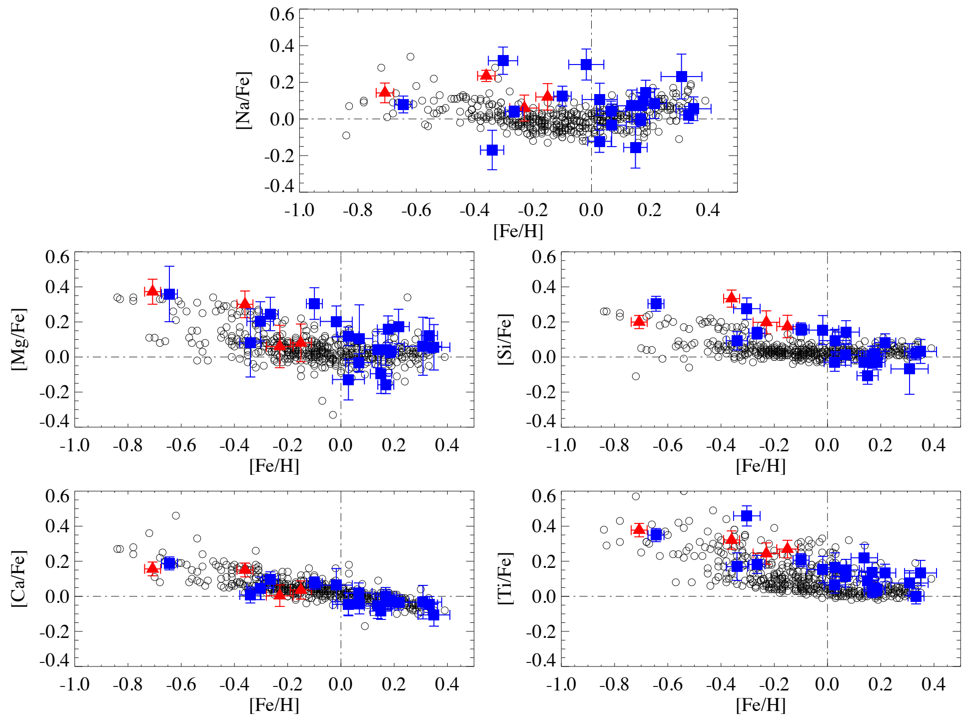

Figure S3 | Stellar abundances of several elements. These element abundances are listed in Supplementary Table S4a relative to iron are compared with the Galactic trends (black circles) of these elements in the relevant range of metallicities[20]. Red triangles correspond to the four giant stars whose distances are marginally compatible with that of the remnant of SN 1006. Blue squares, to the rest of stars in the sample.

Table S1 | Astronomical positions, photometric magnitudes m_R and m_B, and angular distance to the center of the survey, of the sample stars

Name	RA (J2000.0)	DEC (J2000.0)	m_R**	m_B**	d_S [′]
B09472	15:02:56.05	−41:54:52.5	14.9	16.2	0.38
B11408	15:02:58.25	−41:55:21.0	12.5	14.4	0.62
B05723	15:02:51:85	−41:56:39.6	13.7	15.3	1.57
B17720	15:03:05.35	−41:55:33.2	14.8	16.0	1.96
B16564	15:03:04.07	−41:56:34.7	14.3	15.6	2.18
B97338	15:02:42.59	−41:55:36.5	14.7	15.5	2.34
B05518	15:02:51.59	−41:52:49.3	13.8	14.8	2.46
B20292	15:03:08.22	−41:55:18.7	13.5	14.9	2.46
B14130	15:03:01.31	−41:53:01.3	14.5	15.6	2.47
B03395	15:02:49.27	−41:52:21.9	14.8	16.2	3.03
B97341	15:02:42.59	−41:53:11.0	12.9	14.9	3.07
B99810	15:02:45.34	−41:57:48.3	12.3	13.4	3.16
B15360	15:03:02.70	−41:52:19.3	12.6	14.6	3.21
B93571	15:02:38.42	−41:56:10.7	12.4	14.1	3.23
B18024	15:03:05.69	−41:57:48.0	13.7	14.1	3.27
B98824*	15:2:44.23	−41:57:50.7	13.3	14.6	3.32
B08277	15:02:54.72	−41:51:51.5	12.9	14.4	3.34
B24215	15:03:12.42	−41:54:22.1	14.7	16.0	3.38
B14707	15:03:01.92	−41:51:51.5	12.7	14.3	3.58
B90474	15:02:35.04	−41:54:33.1	14.8	16.0	3.77
B90102	15:02:34.64	−41:55:20.6	14.3	15.3	3.79
B10074	15:02:56.75	−41.51:19.1	14.7	15.8	3.89
B95979	15:02:41.10	−41:58:07.8	12.9	13.6	3.91
B09749	15:02:56.39	−41:59:09.0	12.7	13.7	3.96
B21185*	15:03:09.20	−41:52:12.7	13.8	15.3	3.99
B26090	15:03:14.42	−41:56:55.2	12.5	13.2	4.00

*Spectroscopic binary
**0.03 mag uncertainties

Table S2 | Johnson magnitudes m_R, m_B, and 2MASS[19] magnitudes m_J, m_H, m_K, spectral types and luminosity classes[46], and distances of the sample stars

Name	m_R*	m_B*	m_J	m_H	m_K	St. Type**	d [kpc]
B09472	14.9	16.2	14.93±0.05	14.69±0.07	14.55±0.09	G1 V	1.23±0.53
B11408	12.5	14.4	11.05±0.03	10.32±0.03	10.21±0.02	K0-1 III	1.62±0.68
B05723	13.7	15.3	13.63±0.04	13.26±0.05	13.19±0.05	G0-1 V	0.76±0.32
B17720	14.8	16.0	13.61±0.03	13.20±0.03	13.12±0.03	G9-K0 V	0.58±0.25
B16564	14.3	15.6	12.84±0.02	12.22±0.03	12.13±0.02	G9-K0 III	3.03±1.27
B97338	14.7	15.5	13.49±0.02	13.17±0.03	13.09±0.04	G4-5 V	1.05±0.45
B05518	13.8	14.8	13.08±0.03	12.79±0.03	12.72±0.03	F6 V	0.50±0.21
B20292	13.5	14.9	12.40±0.02	11.89±0.02	11.83±0.02	G8 IV	1.13±0.48
B14130	14.5	15.6	13.81±0.03	13.49±0.03	13.51±0.04	F7 V	0.89±0.38
B03395	14.8	16.2	13.76±0.03	13.40±0.03	13.37±0.03	G7 V	0.95±0.41
B97341	12.9	14.9	11.94±0.02	11.38±0.03	11.29±0.02	G9 III	2.48±1.04
B99810	12.3	13.4	11.59±0.02	10.92±0.03	10.82±0.03	K1 III	2.42±1.02
B15360	12.6	14.6	11.43±0.02	10.88±0.02	10.74±0.02	K1 IV	1.29±0.54
B93571	12.4	14.1	10.82±0.02	10.16±0.03	10.01±0.02	K1 III	2.39±1.01
B18024	13.7	14.1	12.88±0.02	12.56±0.03	12.50±0.03	F8-9 V	0.60±0.26
B08277	12.9	14.4	12.20±0.03	11.82±0.02	11.71±0.02	G5 V	0.45±0.19
B24215	14.7	16.0	13.91±0.03	13.51±0.03	13.44±0.04	G4 V	0.95±0.41
B14707	12.7	14.3	11.46±0.02	10.98±0.03	10.88±0.02	K0 IV	1.37±0.58
B90474	14.8	16.0	13.43±0.03	12.91±0.03	12.80±0.03	G6 III	4.78±2.00
B90102	14.3	15.3	13.30±0.02	12.98±0.03	12.86±0.03	G5 V	0.91±0.39
B10074	14.7	15.8	13.46±0.03	13.09±0.02	12.99±0.03	G6 V	0.71±0.30
B95979	12.9	13.6	12.65±0.02	12.52±0.03	12.47±0.03	F1-2 V	0.94±0.40
B09749	12.7	13.7	11.90±0.02	11.60±0.03	11.57±0.03	F7-8 V	0.40±0.17
B26090	12.5	13.2	12.18±0.03	11.89±0.03	11.86±0.03	F8 V	0.37±0.16

*0.03 mag uncertainties
**St. Type refers to spectral type and luminosity class

Table S3 | Photometric distances from different photometric magnitudes and their averages. The error given for each individual distance determination of each photometric magnitude is the 1-σ uncertainty (see text). The errors of the average values are the 1-σ uncertainties associated with the dispersion of the mean from the distances of different magnitudes and the average systematic error, respectively.

Name	d_{m_B} [kpc]	d_{m_R} [kpc]	d_{m_J} [kpc]	d_{m_H} [kpc]	d_{m_K} [kpc]	$d_{\rm av}$ [kpc]
B09472	1.02 ± 0.45	0.95 ± 0.41	1.46 ± 0.62	1.52 ± 0.64	1.46 ± 0.62	$1.23 \pm 0.28 \pm 0.53$
B11408	1.75 ± 0.75	1.67 ± 0.71	1.63 ± 0.69	1.54 ± 0.64	1.52 ± 0.63	$1.62 \pm 0.10 \pm 0.68$
B05723	0.74 ± 0.32	0.59 ± 0.25	0.86 ± 0.36	0.84 ± 0.35	0.84 ± 0.35	$0.76 \pm 0.11 \pm 0.32$
B17720	0.55 ± 0.24	0.60 ± 0.26	0.58 ± 0.25	0.59 ± 0.25	0.58 ± 0.25	$0.58 \pm 0.02 \pm 0.25$
B16564	2.78 ± 1.19	3.31 ± 1.40	3.11 ± 1.30	3.00 ± 1.24	2.98 ± 1.23	$3.03 \pm 0.19 \pm 1.27$
B97338	0.97 ± 0.42	1.17 ± 0.50	1.04 ± 0.44	1.05 ± 0.44	1.04 ± 0.44	$1.05 \pm 0.07 \pm 0.45$
B05518	0.51 ± 0.22	0.50 ± 0.21	0.51 ± 0.21	0.50 ± 0.21	0.50 ± 0.21	$0.50 \pm 0.01 \pm 0.21$
B20292	1.09 ± 0.47	1.13 ± 0.48	1.15 ± 0.48	1.13 ± 0.47	1.13 ± 0.47	$1.13 \pm 0.02 \pm 0.48$
B14130	0.89 ± 0.39	0.85 ± 0.36	0.90 ± 0.38	0.88 ± 0.37	0.91 ± 0.38	$0.89 \pm 0.02 \pm 0.38$
B03395	0.99 ± 0.43	0.94 ± 0.40	0.93 ± 0.40	0.94 ± 0.40	0.96 ± 0.41	$0.95 \pm 0.02 \pm 0.41$
B97341	2.59 ± 1.10	2.21 ± 0.94	2.58 ± 1.08	2.55 ± 1.05	2.54 ± 1.05	$2.48 \pm 0.16 \pm 1.04$
B99810	1.59 ± 0.68	2.22 ± 0.95	3.08 ± 1.30	2.98 ± 1.25	2.96 ± 1.23	$2.42 \pm 0.67 \pm 1.02$
B15360	1.48 ± 0.63	1.23 ± 0.52	1.28 ± 0.54	1.26 ± 0.52	1.23 ± 0.51	$1.29 \pm 0.11 \pm 0.54$
B93571	2.34 ± 1.00	2.54 ± 1.08	2.42 ± 1.02	2.38 ± 0.99	2.30 ± 0.96	$2.39 \pm 0.09 \pm 1.01$
B18024	0.48 ± 0.21	0.65 ± 0.28	0.65 ± 0.27	0.64 ± 0.27	0.64 ± 0.27	$0.60 \pm 0.07 \pm 0.26$
B08277	0.47 ± 0.21	0.42 ± 0.18	0.47 ± 0.20	0.46 ± 0.19	0.45 ± 0.19	$0.45 \pm 0.02 \pm 0.19$
B24215	0.96 ± 0.42	0.92 ± 0.39	0.98 ± 0.41	0.96 ± 0.40	0.96 ± 0.40	$0.95 \pm 0.02 \pm 0.41$
B14707	1.41 ± 0.61	1.38 ± 0.58	1.36 ± 0.57	1.36 ± 0.56	1.34 ± 0.56	$1.37 \pm 0.03 \pm 0.58$
B90474	4.43 ± 1.89	5.22 ± 2.21	4.87 ± 2.03	4.77 ± 1.97	4.70 ± 1.94	$4.78 \pm 0.29 \pm 2.00$
B90102	0.84 ± 0.37	0.94 ± 0.40	0.92 ± 0.39	0.94 ± 0.40	0.92 ± 0.39	$0.91 \pm 0.04 \pm 0.39$
B10074	0.72 ± 0.31	0.78 ± 0.33	0.69 ± 0.29	0.69 ± 0.29	0.68 ± 0.29	$0.71 \pm 0.04 \pm 0.30$
B95979	0.81 ± 0.36	0.84 ± 0.36	1.01 ± 0.42	1.04 ± 0.43	1.03 ± 0.43	$0.94 \pm 0.11 \pm 0.40$
B09749	0.40 ± 0.18	0.40 ± 0.17	0.41 ± 0.17	0.40 ± 0.17	0.41 ± 0.17	$0.40 \pm 0.00 \pm 0.17$
B26090	0.29 ± 0.13	0.34 ± 0.14	0.43 ± 0.18	0.43 ± 0.18	0.43 ± 0.18	$0.37 \pm 0.07 \pm 0.16$

Table S4a | Abundance ratios [X/Fe] of the sample stars in the SN 1006 survey for Na and the α-elements Mg, Si, Ca and Ti. The errors provide the 1-σ uncertainties associated with the dispersion of the measurements from different spectral features.

Name	[Na/Fe]	[Mg/Fe]	[Si/Fe]	[Ca/Fe]	[Ti/Fe]
B09472	0.30 ± 0.08	0.20 ± 0.09	0.14 ± 0.18	0.06 ± 0.21	0.17 ± 0.18
B11408	0.32 ± 0.08	0.20 ± 0.14	0.28 ± 0.11	0.05 ± 0.11	0.43 ± 0.13
B05723	0.23 ± 0.00	0.06 ± 0.21	-0.07 ± 0.28	-0.03 ± 0.09	0.08 ± 0.03
B17720	0.06 ± 0.04	0.06 ± 0.16	0.01 ± 0.18	-0.11 ± 0.07	0.11 ± 0.17
B16564	0.24 ± 0.01	0.30 ± 0.10	0.34 ± 0.12	0.15 ± 0.08	0.31 ± 0.17
B97338	-0.12 ± 0.06	0.45 ± 0.42	-0.03 ± 0.11	-0.05 ± 0.14	0.07 ± 0.10
B05518	-0.16 ± 0.15	-0.10 ± 0.15	-0.11 ± 0.08	-0.08 ± 0.07	0.07 ± 0.14
B20292	0.08 ± 0.05	0.30 ± 0.26	0.30 ± 0.09	0.19 ± 0.06	0.36 ± 0.09
B14130	0.02 ± 0.05	0.12 ± 0.13	0.01 ± 0.07	-0.05 ± 0.10	0.02 ± 0.13
B03395	0.08 ± 0.00	0.17 ± 0.13	0.07 ± 0.06	-0.03 ± 0.04	0.13 ± 0.12
B97341	0.12 ± 0.08	0.08 ± 0.00	0.20 ± 0.16	0.04 ± 0.10	0.24 ± 0.11
B99810	0.14 ± 0.06	0.37 ± 0.09	0.20 ± 0.07	0.16 ± 0.08	0.38 ± 0.13
B15360	-0.03 ± 0.15	0.20 ± 0.40	0.17 ± 0.16	-0.04 ± 0.09	0.14 ± 0.15
B93571	0.06 ± 0.07	0.06 ± 0.16	0.22 ± 0.14	0.00 ± 0.10	0.22 ± 0.15
B18024	-0.17 ± 0.00	0.08 ± 0.27	0.08 ± 0.11	0.01 ± 0.06	0.20 ± 0.26
B08277	0.14 ± 0.08	0.03 ± 0.02	-0.03 ± 0.09	-0.03 ± 0.07	0.04 ± 0.06
B24215	0.07 ± 0.08	0.04 ± 0.11	0.01 ± 0.08	-0.00 ± 0.09	0.11 ± 0.15
B14707	0.10 ± 0.02	0.16 ± 0.09	0.03 ± 0.09	-0.03 ± 0.03	0.09 ± 0.14
B90474	0.04 ± 0.01	0.25 ± 0.13	0.18 ± 0.09	0.10 ± 0.09	0.16 ± 0.19
B90102	0.12 ± 0.06	0.30 ± 0.12	0.16 ± 0.05	0.08 ± 0.05	0.21 ± 0.08
B10074	0.04 ± 0.03	-0.03 ± 0.01	0.01 ± 0.09	0.02 ± 0.08	0.10 ± 0.14
B95979	0.11 ± 0.09	-0.24 ± 0.00	0.09 ± 0.06	-0.05 ± 0.07	0.15 ± 0.18
B09749	0.07 ± 0.00	0.04 ± 0.13	-0.05 ± 0.11	-0.06 ± 0.14	0.22 ± 0.23
B26090	-0.00 ± 0.02	-0.16 ± 0.06	-0.03 ± 0.07	-0.00 ± 0.07	0.03 ± 0.06

Table S4b | Abundance ratios [X/Fe] (cont.) of the sample stars in the SN 1006 survey for the iron-peak elements Cr, Mn, Co and Ni.

Name	[Cr/Fe]	[Mn/Fe]	[Co/Fe]	[Ni/Fe]
B09472	0.14 ± 0.21	-0.10 ± 0.10	0.03 ± 0.21	0.07 ± 0.12
B11408	-0.00 ± 0.15	-0.03 ± 0.21	0.28 ± 0.10	0.08 ± 0.11
B05723	-0.09 ± 0.11	0.22 ± 0.22	0.17 ± 0.12	0.03 ± 0.19
B17720	-0.11 ± 0.09	0.22 ± 0.31	0.17 ± 0.12	0.07 ± 0.10
B16564	-0.03 ± 0.16	0.01 ± 0.10	0.38 ± 0.18	0.09 ± 0.10
B97338	-0.08 ± 0.12	0.00 ± 0.09	-0.01 ± 0.13	-0.03 ± 0.12
B05518	-0.11 ± 0.08	-0.04 ± 0.16	-0.19 ± 0.13	0.00 ± 0.12
B20292	0.00 ± 0.15	-0.15 ± 0.15	0.18 ± 0.06	0.03 ± 0.10
B14130	-0.03 ± 0.08	0.12 ± 0.16	-0.01 ± 0.09	0.06 ± 0.07
B03395	-0.07 ± 0.05	0.14 ± 0.29	0.17 ± 0.06	0.07 ± 0.07
B97341	-0.04 ± 0.23	0.07 ± 0.09	0.27 ± 0.12	0.03 ± 0.10
B99810	-0.01 ± 0.18	-0.15 ± 0.08	0.15 ± 0.14	0.04 ± 0.12
B15360	-0.06 ± 0.10	0.14 ± 0.21	0.32 ± 0.28	0.09 ± 0.12
B93571	0.04 ± 0.08	-0.18 ± 0.20	0.23 ± 0.17	0.04 ± 0.15
B18024	-0.01 ± 0.27	-0.12 ± 0.12	0.05 ± 0.29	-0.05 ± 0.13
B08277	-0.02 ± 0.07	0.14 ± 0.13	0.10 ± 0.13	0.03 ± 0.06
B24215	-0.06 ± 0.12	0.02 ± 0.07	0.11 ± 0.11	0.06 ± 0.11
B14707	-0.09 ± 0.12	0.31 ± 0.11	0.14 ± 0.12	0.01 ± 0.13
B90474	-0.11 ± 0.14	-0.02 ± 0.16	0.23 ± 0.19	-0.00 ± 0.09
B90102	-0.04 ± 0.14	-0.14 ± 0.05	0.14 ± 0.12	0.04 ± 0.09
B10074	-0.04 ± 0.09	0.06 ± 0.08	0.06 ± 0.11	0.03 ± 0.11
B95979	-0.06 ± 0.19	-0.09 ± 0.25	-0.11 ± 0.27	-0.05 ± 0.23
B09749	0.05 ± 0.16	-0.06 ± 0.20	0.05 ± 0.21	0.06 ± 0.09
B26090	-0.05 ± 0.10	0.03 ± 0.05	-0.05 ± 0.10	-0.02 ± 0.07